# **Dual Polarized Reconfigurable MIMO Antenna for Multi-Band Functioning**

# T. Vijetha<sup>1</sup>, D. Ramakrishna<sup>2</sup>, and K. Bharath<sup>2</sup>

<sup>1</sup> Department of ECE, MLR Institute of Technology, Hyderabad, India

Corresponding author: T.Vijetha (e-mail: Vijetha.tummala@mlrinstitutions.ac.in).

ABSTRACT This work presents the design, development and measurements of a novel Multi-Band Frequency Reconfigurable MIMO Active Integrated Antenna (AIA) with Ultra-Wideband sensing capabilities. The antenna comprises two planar inverted F-shape antennas (PIFA) utilizing meandered line (ML) structures and a UWB sensing antenna with a mirror-shaped configuration. Integrated with 2x2 MIMO Meandered line PIFA elements for spectrum sensing, the antenna employs PIN diodes (BAR 6402V) for digital switching, enabling frequency reconfigurability, and varactor diodes for wideband tuning. PIN diodes (BAR 6402V) are used to provide all digital switching on/off combination modes to attain frequency reconfigurability. Varactor diodes are used for tuning over the wide band. The proposed antenna effectively senses a wide frequency band from 0.5GHz-3GHz and offering frequency reconfigurability over the five bands based on BARP6402V switching modes (0.78GHz-1.01GHz, 1.34GHz-1.62GHz, 1.85GHz-2.18GHz, 2.44GHz-2.67GHz, and 2.76GHz-2.80GHz). Fabricated on an FR4 substrate measuring 120mmX65mmX1.6mm, the antenna achieves a high gain of 6.15dBi at a frequency of 1.75GHz. Performance parameters obtained from measurements are compared with simulated results. The research comprehensively analyzes 2x2 MIMO parameters, including Total Active Reflection Coefficient (TARC), Isolation coefficient, Envelope Correlation Coefficients (ECC), Diversity Gain (DG), Multiplexing efficiency, among others. The proposed antenna demonstrates stability, excellent gain, and an omnidirectional radiation pattern across desired bands, making it suitable for applications such as sensing, communication, UWB sensing, and cognitive radio (CR). Its reconfigurable nature also extends its utility to various general-purpose applications, including GPS tracing, LTE, UMTS, GSM1800, rescue operations, Wi-Fi/Bluetooth/ISM/WLAN, CDMA, and more

**INDEX TERMS** Active Integrated Antenna, Cognitive radio, Frequency reconfigures, MIMO antenna, MIMO parameters, multi-band, PIN diodes, UWB sensing, Varactor diodes.

# I. INTRODUCTION

The Antennas serve as crucial components for various applications, such as microstrip to rectangular waveguide transitions, transmitter/receivers, filtering antennas (filtennas), rectennas, and more [1-3]. The evolution of low-cost antennas has been driven by innovations in fractals, metamaterials, Electromagnetic Band Gap (EBG) structures, and meandered lines [4]. In recent years, the focus of researchers has shifted towards Multiple Inputs Multiple Outputs (MIMO), Frequency Reconfigurable (FR), and sensing antennas, particularly Ultra-Wideband (UWB) sensing antennas for Cognitive Radio (CR) applications [5-13].

Cognitive Radio involves smart radio systems that intelligently capture and communicate signals based on software-defined programs, operating in the frequency range below 3GHz. To achieve effective sensing in this range, integrating a frequency-reconfigurable antenna with a UWB-sensing multiband antenna becomes essential. This paper explores the hybrid combination of a reconfigurable antenna and a UWB sensing antenna in the context of CR. Previous designs in this realm include a 4x4 MIMO system by Hussain et al., utilizing varactor diodes for tuning and

achieving a radiation efficiency of 81% [5]. Dhar et al. presented an active antenna combining MIMO and an amplifier for UWB sensing, demonstrating a peak gain of 14.1 dBi and a radiation efficiency of 60% [6]. As 4G/5G and 6G wireless communication advance, MIMO antennas play a vital role in high-speed data transfer, utilizing configurations like monopole ground MIMO, reconfigurable MIMO, Massive MIMO, and millimeter-wave MIMO [12]. Various designs, such as those proposed by Chamok et al. for gain improvement in wireless handheld devices, showcase the versatility of antenna arrays [14]. The paper further discusses pattern reconfigurable MIMO antennas, such as the design by Li et al., achieving radiation efficiency of 85% at 2.65GHz using PIN diodes and a decoupling mechanism [15]. Additionally, frequency reconfigurable MIMO antennas for WLAN and UMTS operations, as presented by Hussain et al., are explored, demonstrating peak gains and radiation efficiencies [16, 17]. Further contributions include a phased array antenna system with wide-angle scanning by Haider et al. [18], a pattern reconfigurable antenna using a cylindrical dielectric antenna resonator by Liu et al. [19], and a compact frequency-

<sup>&</sup>lt;sup>2</sup> Department of ECE, Osmania University, Hyderabad, India



reconfigurable filtenna by Tang et al. with Varactor diodes for narrow and wide-band frequency coverage [20].

The paper is organized as follows: section-1 discussed the recent MIMO antenna configurations with ultra-wideband frequency range. Secion-2 mentioned the recent multi-band UWB sensing antennas with their goods and shortcoming. And hence discusses the aims and objectives of the proposed work. Section-3 explained the proposed design geometry development and its prototype fabrication method in brief. Section-4 discussed the different switching modes of PIN diodes and Varactor diodes results and their measurements. It also explains the state-of-art of the proposed design over the existing method. Section-5 concluded the research work with future scope.

# **II. LITERATURE SURVEY**

Zhao et al., have proposed a UWB MIMO reconfigurable antenna for CR applications. It consists of two MIMO antennas to achieve the frequency reconfigurability in UWB range from 1 to 4.5 GHz. The antenna geometry combines a modified triangular shape, a semi-circular ring, and a rectangular patch-printed monopole antenna. The PIN diode switching modes cover a UWB frequency range from 1 GHz to 4.5 GHz, while Varactor diode switching modes operate the main antenna between 0.9 GHz and 2.6 GHz. The MIMO isolation factor is below -12.5 dB, and the envelope correlation coefficient (ECC) remains below 0.19 for all resonant frequencies [7].

Hussain and Sharawai introduced an integrated slot-linebased frequency reconfigurable antenna system with four elements sensing the UWB frequency range from 1 GHz to 6 GHz. Each sensing element consists of a unique split-ring oscillator and half-annular slots operating in tri-bands. Varactor diodes provide tuning for each antenna element, resulting in a total frequency range of 1.48-4.56 GHz. Fabricated on an RO-4350 substrate, the antenna achieves a radiation gain of 4.2 dBi and radiation efficiency above 81% [13]. Vijetha et al. proposed a combination of frequencyreconfigurable and UWB sensing 2X2 MIMO antenna. The UWB sensing antenna operates in the frequency range of 720 MHz-3440 MHz, while PIN diodes enable frequency reconfiguration in the range of 0.573 MHz-2.55 MHz. Varactor diodes tune the frequency band of 720 MHz-3440 MHz at resonant frequencies of 1.10 GHz and 2.48 GHz. The designed antenna, with symmetric inline meandered line PIFA, is suitable for wireless hand-held, CR, and WLAN applications, although MIMO analysis is not discussed [13].

Hussain et al. designed a frequency-reconfigurable 4X4 MIMO antenna using a concentric pentagonal-slotted shape on an FR-4 substrate for UWB frequency range sensing. The antenna utilizes 8 Varactor diodes, with only two connected in each slotted pentagon shape to provide an adjustable frequency range. Two sensing elements cover a UWB frequency range from 1.32 GHz to 1.49 GHz, while the other two cover 1.75 GHz to 5.2 GHz. The antenna achieves a peak gain of 4.5 dBi and a radiation efficiency of 81%, with an ECC lower than 0.186 for all resonant frequencies, making it suitable for CR-enabled applications [21].

Sumana et al. demonstrated a shape memory alloy for the bottom ground plane in an antenna, achieving frequency reconfigurability in UWB sensing CR applications from 3.4 GHz to 10.2 GHz. The antenna uses rectangular slits for dual-band operation from 4.7 GHz to 6.0 GHz, achieving a voltage standing wave ratio <2 and a reflection coefficient of <-10 dB in all modes. The innovative shape memory alloy technique simplifies design and eliminates the need for complex excitation circuitry [22].

Xing et al. presented a water dielectric resonator antenna for frequency reconfiguration in VHF and UHF ranges. The operating frequency range depends on the water height, covering quad bands from 168 MHz to 474 MHz. The antenna achieves radiation efficiency higher than 81% [23]. Zhang et al. introduced an 8X8 MIMO antenna with frequency reconfigurability for UWB sensing in 5G network smartphones. Each antenna element is powered by a microstrip line with a tuning stub, operating in the frequency range from 3.3 GHz to 6 GHz with an isolation lower than -11 dB. The antenna achieves a minimum ECC of 0.09 in all resonant frequency ranges [24]. Ghaffar et al. proposed a multimode antenna using a triangular shape printed monopole antenna with two PIN diodes for frequency reconfigurability. The antenna operates in 4G-LTE, ISM, 5G-sub, and S-bands, achieving a peak gain of 2.72 dBi [25].

Hussain et al. designed a miniaturized meandered slot-line-based frequency reconfigurable 2X2 MIMO antenna for UWB sensing. Two sensing elements, connected in the H-shaped, use a Varactor diode for quad-band frequency reconfiguration in the range of 0.665-1.13 GHz, 1.415-2.005 GHz, 2.42-3.09 GHz, and 3.18-3.89 GHz, covering a total frequency range of 1.48-4.56 GHz. The antenna, fabricated on an RO-4350 substrate, has a radiation efficiency of 83% and an ECC below 0.078 for efficient MIMO operation [26].

Thummalaru et al. proposed a frequencyreconfigurable filtenna with five diodes and three switching modes for 5G ultra-wideband. Varactor diodes are used to select specific frequencies in the range of 2.5-4.2 GHz, achieving a minimum envelope correlation coefficient value for a 4X4 MIMO system [27]. Yuan et al. designed an antenna using T-shaped and C-shaped slots on the metal frame, an inverted L-shaped microstrip line, and an H-shaped resonator for decoupling in an 8X8 MIMO system. The antenna senses a frequency range from 3.3 GHz to 6 GHz, achieving an ECC of <0.05 and a radiation efficiency of >40% [28].In a circular monopole antenna, the most intense current is around the periphery, allowing for a reduction in the central portion without significantly affecting performance [12]. Building upon this concept, a hybrid combination of circular and rectangular patches gives rise to a new mirrorshaped slotted antenna. This slotted mirror-shaped antenna senses the UWB frequency range from 0.5 GHz to 3 GHz, while Varactor diodes enable UWB sensing at five different bands.

The present research introduces a compact, reliable frequency-reconfigurable MIMO antenna designed for multiband operation, incorporating a slotted mirror-shaped antenna for UWB tuning in the frequency range of 0.5 GHz to 3.0 GHz. The primary objectives of this method are to design an efficient frequency-reconfigurable antenna operating in

multiband PIN digital switching modes below 3 GHz, with a miniaturized substrate volume and excellent performance. This is achieved by switching the PIN diode parasitic elements in the MIMO antenna. The work addresses the previous challenge of poor decoupling between MIMO elements by employing an off-set PIFA element placement on the bottom side, aiming to improve the isolation coefficient and overall MIMO performance. Additionally, the design incorporates separate biasing circuits for PIN diodes and Varactor diodes to enhance impedance matching characteristics by reducing parasitic loading effects

#### III. DESIGN METHODOLOGY

#### A. Reconfigurable MIMO Antenna Geometry

The proposed Ultra-Wideband (UWB) sensing reconfigurable Active Integrated Antenna (AIA) is meticulously designed and fabricated on an FR4 substrate with a dielectric constant of 4.4, a loss tangent of 0.02, and dimensions measuring 65mm x 120mm x 1.6mm, as illustrated in Fig. 1. The top side of the substrate features a monopole hybrid UWB sensing slotted mirror-shaped quarter-wave transformer-fed antenna, while the bottom side showcases a 2x2 Multiple Input Multiple Output (MIMO) antenna, as depicted in Fig. 1(a-b). The UWB sensing antenna employs a reduced squareshape ground with dimensions of 25mm x 25mm. On the bottom side, the 2x2 MIMO planar inverted F-antenna (PIFA element) utilizes a meandered line. Subsequently, the meandered line MIMO antenna, with an inverted F-shape, undergoes frequency reconfiguration using two BAR6402V and two Varactor diodes (SOD 323) for UWB-tuning. The UWB sensing antenna serves as the ground for the two MIMO antennas. Fig. 1(a-c) provides a comprehensive dimensional representation (in mm) of the antenna's geometrical structure. The  $50\Omega$  feed has a width (W<sub>f</sub>) of 3mm and a length (L<sub>f</sub>) of 4mm. The impedance of the 1.5mm x 31mm (W<sub>t</sub> x L<sub>t</sub>) impedance matching transformer is  $73\Omega$ , while the impedance of the slotted mirror patch is  $110\Omega$ . The guided wavelength at the design frequency of 1.75GHz is calculated as 81.66mm. Consequently, the impedance and width of the impedance and width of the impedance transformer are determined by using the following relationships [12].

$$\underline{Z_{\frac{\lambda_g}{4}}} = \sqrt{\left(Z_0 \cdot Z_{\text{patch}}\right)} \tag{1}$$

 $Z_0$ =impedance of the Feed,  $50\Omega$ 

 $Z_P$ =impedance of the slotted patch, 110 $\Omega$ . And

$$\begin{split} & \text{For}\!\left(\!\frac{W_t}{h}\!\right) < 1; \\ & Z_{\!\frac{\lambda_g}{4}} = \frac{60}{\sqrt{(\epsilon_{\text{eff}})}} \ln\!\left(8\left(\!\frac{h}{W_t}\!\right) + 0.25\left(\!\frac{W_t}{h}\!\right)\!\right) \end{split} \tag{2}$$

$$\varepsilon_{\text{eff}} = \frac{\varepsilon_{\text{r}} + 1}{2} + \frac{\varepsilon_{\text{r}} + 1}{2} \left[ \frac{1}{\sqrt{1 + 12\left(\frac{h}{W_{\text{t}}}\right)}} + 0.04\left(1 - \left(\frac{W_{\text{t}}}{h}\right)^2\right) \right]$$
(3)

The quarter wavelength of the evaluated impedance transformer is 24.2mm, while the simulated optimized length (Lt) is 31.0mm. The UWB sensing antenna is positioned on the top layer of the substrate, featuring a mirror-shaped structure derived from a circular monopole antenna to achieve a wideband characteristic, with dimensions of 75mm x 47mm. The width (WP) and length (LP) of the UWB sensing rectangular patch antenna are determined using standard relationships derived from equations (4-10) [1]. The width of the patch is 47.0mm, and the length is 75mm. A central portion with an area of mm<sup>2</sup> has been eliminated from the rectangular patch, with an upper two-filleted corner having a radius (R fillet) of 15mm, as illustrated in Fig. 1(a).

Height of the substrate 
$$h \leq \frac{0.3c}{2\pi f\sqrt{\epsilon_{\rm p}}} \tag{4}$$

f is the frequency in GHz, c velocity of light, Er relative permittivity.

Width of meandered line

$$W_{p} = \frac{c}{f} \sqrt{\frac{2}{\epsilon_{r}+1}} \tag{5}$$

Length of meandered line 
$$L_p = \frac{c}{2f\sqrt{\epsilon_p}ff} - 2\Delta l \tag{6}$$

 $\Delta$ l=Physical Length,  $\varepsilon_{eff}$  effective permittivity

$$\varepsilon_{\text{eff}} = \frac{\varepsilon_{\text{r}} + 1}{2} + \frac{\varepsilon_{\text{r}} - 1}{2} \left( \sqrt{1 + \frac{12h}{w_2}} \right)^{-1} \tag{7}$$

$$\Delta l = \frac{0.412h(\epsilon_{eff} + 0.3)(\frac{w_2}{h} + 0.262)}{(\epsilon_{eff} - 0.258)(\frac{w_2}{h} + 0.813)} \tag{8}$$

Width of the substrate

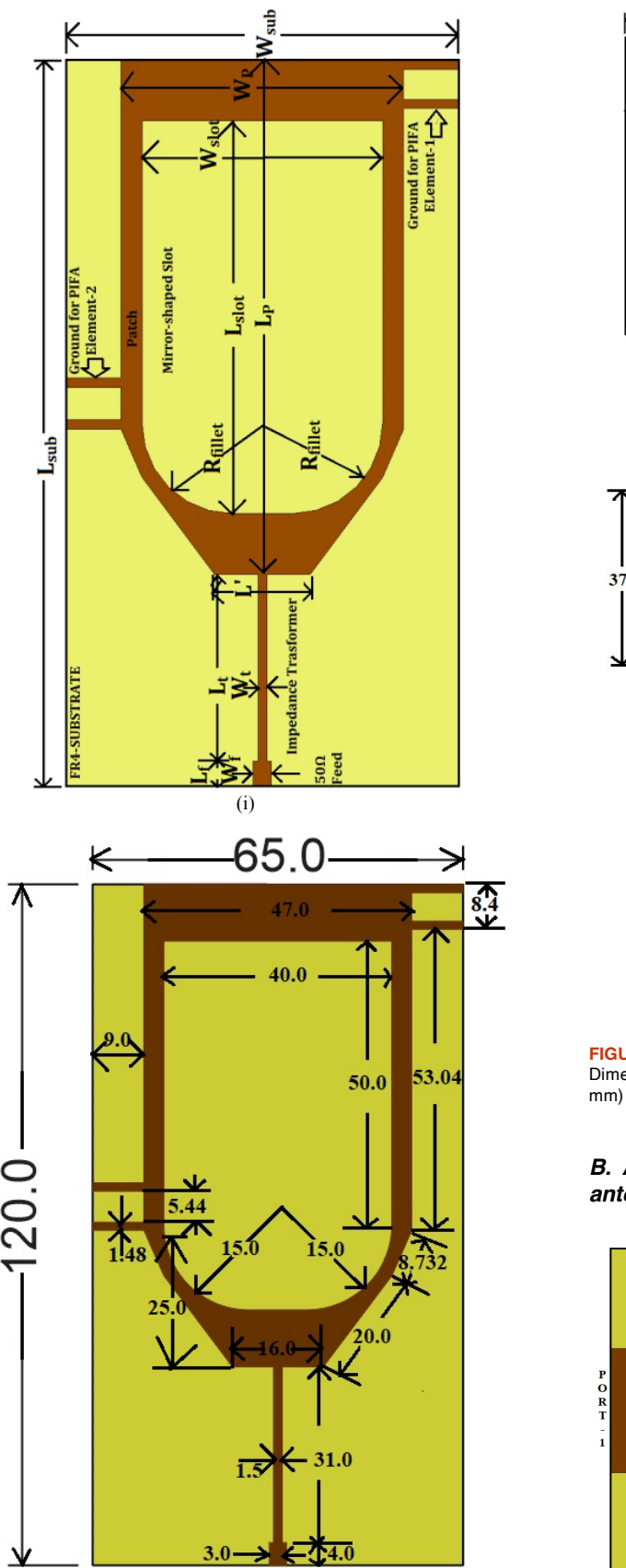
$$W_{\text{sub}} = W_{\text{p}} + 6h \tag{9}$$

Length of the substrate

$$\mathbf{L_{sub}} = \mathbf{L_p} + 6\mathbf{h} \tag{10}$$

On the bottom surface of the substrate, the two antennas are positioned at an offset spatial distance (D) of 49.2mm. The width of the meander line elements is 1.48mm, matching the width of the Planar Inverted F-Antenna (PIFA). Both inverted-F arms are separated by a distance of 5.44mm. The simulated optimized length values of the meander lines are W1=56.6mm, W2=43.70mm, and W3=38.96mm. The inverted F-arm length W4=9.0mm is precisely equal to the first fold length of the meander line. Another fold length of the meandered line is 4.96mm.





(ii)

(a)

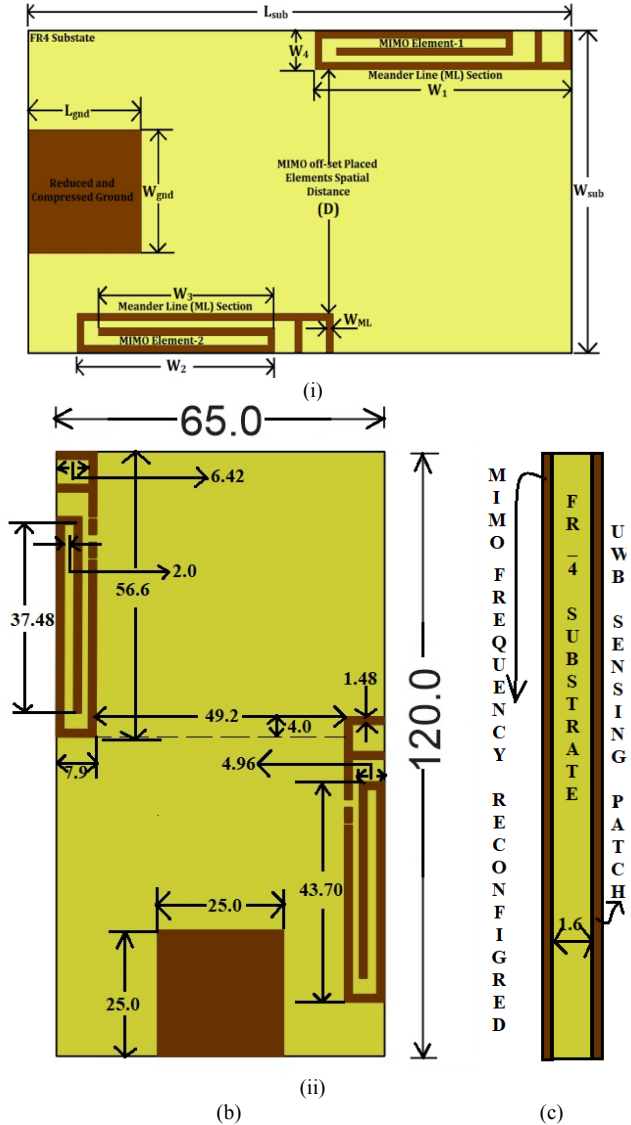
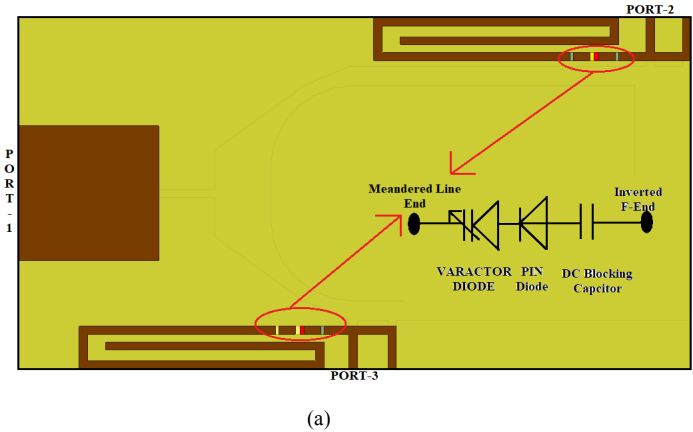


FIGURE 1. UWB sensing using MIMO antenna (a) (i) Parametric Top view, (ii) Dimensions (in mm) and (b) (i) Parametric Bottom View, (ii) Dimensions (in mm) (c) Side view.

# B. Attachment of Varactor and PIN diodes in meander antenna arms





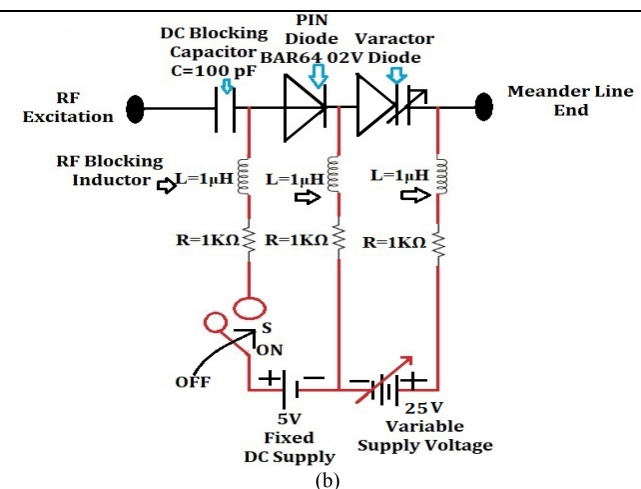


FIGURE 2. Arrangement of PIN and Varactor diodes for the biasing Circuit (a) UWB sensing MIMO antenna With PIN and Varactor connections (b) Separated Power Supply for both MIMO sections PIN diode and Varactor diode Biasing

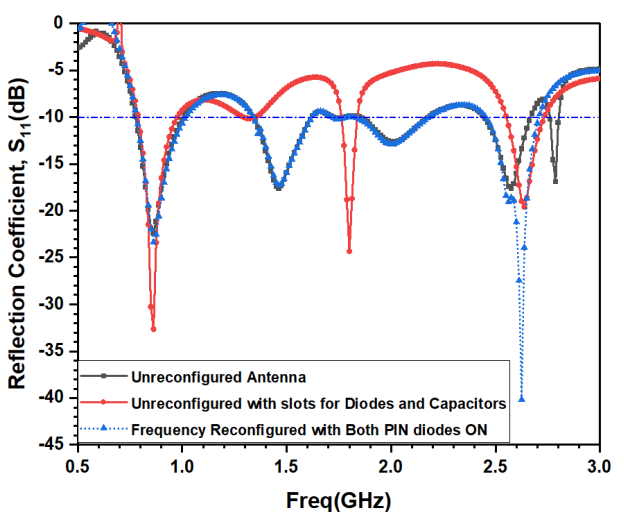


FIGURE 3. Un-reconfigured and frequency reconfigured UWB sensing

In the un-frequency reconfigured Ultra-Wideband (UWB) sensing with the Multiple Input Multiple Output (MIMO) antenna from the previous section, slots at optimized locations are cut for the connection of the DC blocking capacitors, PIN diodes, and Varactor diodes, and then soldered at the appropriate locations with care to avoid shorting pins. Subsequently, all possible digital logical switching conditions for ON/OFF of BAR6402V with a 5V DC power supply and biasing circuits have been applied. A 100pF DC blocking capacitor is used to prevent unwanted DC signals from the RF excitation end, and 1µH RF chokes are employed to block any AC signals in the DC power supply from a protection standpoint. Varactor diodes operate in reverse bias conditions, and their capacitor value decreases with an increase in variable DC voltage. Therefore, Varactors are kept in reverse bias with a 25V variable power supply. The connection arrangement of PIN and Varactor diodes is shown in Fig. 2 (a), and their power supply/biasing circuit arrangement is illustrated in Fig. 2 (b). This biasing circuit is connected to two symmetric offset meandered line structures on the bottom layer of the antenna, consisting of one PIN or Varactor in a series combination with a radio choke of 1 µH and a series resistor of  $1K\Omega$  that connects the PIN and

Varactor diode to the radiating elements of the MIMO antenna. The series connection of diodes with an RF choke helps isolate the bias circuit from the antenna. The reflection coefficient (S11) without slot cuts, with slot cuts, and after the insertion of Varactor diodes, PIN diodes, and blocking capacitors with power supply is presented in Table-I and compared in Fig. 3. The recorded results indicate that initially, the UWB sensing MIMO antenna has five narrow bands below -10dB. As slots for the Varactor diodes, PIN diodes, and DC blocking capacitors are introduced in the meander lines of the MIMO elements, the UWB sensing antenna resonates at three frequencies in three narrow bands. With the connection of PIN diodes, a Varactor diode, and a DC blocking capacitor at the slots, the antenna exhibits quad resonating bands below -10dB reflection coefficients (S11) values. Comparing the reconfigured antenna with the unreconfigured antenna reveals improvements in the reflection coefficient values at resonance frequencies. The first three resonance frequencies are unaffected by the connection of PIN diodes in ON conditions, while the fourth resonance frequency shifts towards the left by 160MHz, resulting in an improved bandwidth below -10dB reflection coefficients. At the third resonance frequency, there is also an improvement in the -10dB bandwidth. In terms of gain, frequency reconfigurability also contributes to an improvement in the gain of un-reconfigured antenna

TABLE I. Un-reconfigured and frequency-reconfigured UWB sensing antenna

Mode of Operation	<b>f</b> <sub>r</sub> (GHz)	-10dB Bands f <sub>L</sub> - f <sub>H</sub> (GHz)	<b>S</b> <sub>11</sub> (dB)	G (dBi)
Un- Reconfigured	0.86 1.47 2.01 2.57 2.79	0.78-1.01, 1.34-1.62, 1.85-2.18, 2.44-2.67, 2.76-2.80	-22.30, -17.56, -12.67, -17.64, -16.82	5.80, 3.45, -10.26, 4.07, 20.44
Un- reconfigured with Slots	0.86, 1.80, 2.64	0.79-0.98, 1.76-1.84, 2.55-2.73	-32.61, -24.33, -19.55	6.36, -0.38, 0.75
Reconfigured (Both PIN diodes ON)	0.86, 1.46, 2.0, 2.63	0.78-1.02, 1.34-1.62, 1.72-2.18, 2.45-2.71	-23.33, -17.28, -12.90, -40.18	7.27, 3.85, -10.58, 18.18

# C. Effect of Meander Line Sections on UWB Sensing Antenna

The impact of inserting an offset-located symmetric meander line inverted F-shaped structure in the monopole Ultra-Wideband (UWB) sensing antenna and the mirror-shaped UWB sensing antenna without meander line insertion is compared in Fig. 4. It is observed from the recorded values in Table-II that the antenna without the parasitic meander line exhibits a dual-band nature with very high gain, measuring 17.79 dBi and -4.38 dBi at resonance frequencies of 0.83GHz and 2.64GHz, respectively. After loading with a parasitic inverted F-shaped structure with a folded meander line, the UWB sensing antenna's reflection coefficient becomes quadband in nature, with a reduction in gain values as depicted in Table II.

VOL. 13, NO. 2, JULY 2024 5



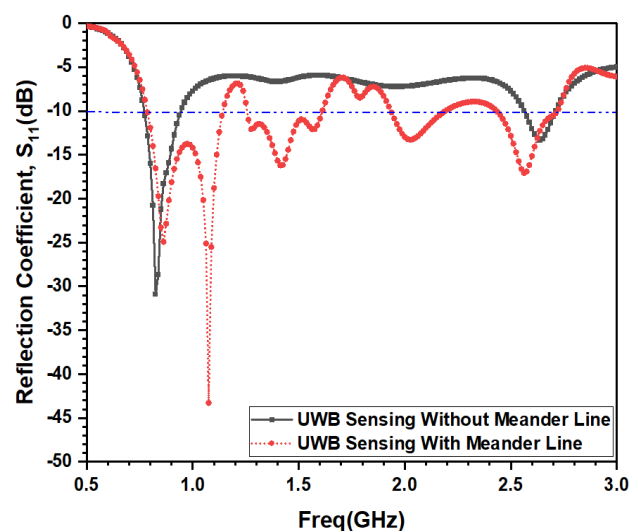


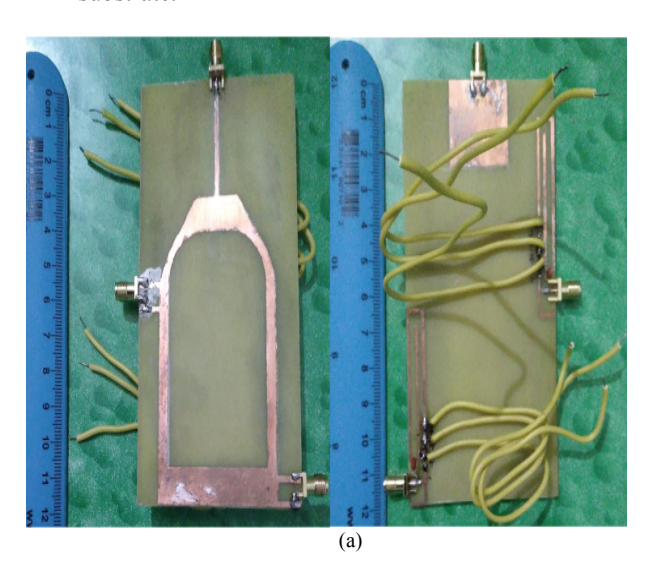
FIGURE 4. UWB sensing with the addition of ML

TABLE II. Un-reconfigured and frequency-reconfigured UWB sensing antenna

Mode of Operation	f <sub>r</sub> (GHz)	-10dB Bands f <sub>L</sub> - f <sub>H</sub> (GHz)	<b>S</b> <sub>11</sub> (dB)	G (dBi)	
(UWB Sensing)					
Antenna	0.83,	0.77-0.94,	-30.91,	17.79,	
without	2.64	2.56-2.71	-13.30	-4.38	
Meander Line					
Antenna with	0.86 &	0.79-1.14,	-32.61 & -	7.98 &	
Meander Line	1.07,		43.30,	3.62,	
	1.42,	1.26-1.61,	-16.20,	5.06,	
	2.02,	1.93-2.19,	-13.29,	-9.09,	
	2.57	2.43-2.72	-16.94	3.04	

# D. UWB Sensing Active Antenna Prototype

A double-sided fabricated prototype of a mirror-shaped slotted Ultra-Wideband (UWB) sensing antenna with a 2x2 Multiple Input Multiple Output (MIMO) symmetrical element arrangement at an offset location has been displayed in Fig. 5. Finally, three  $50\Omega$  SMA connectors are soldered, along with two PIN diodes (BAR6402V), two Varactor diodes (SOD 323), and two DC blocking capacitors (100 pF) [29]. Two separate power supplies are integrated on a single-layered FR4 substrate.



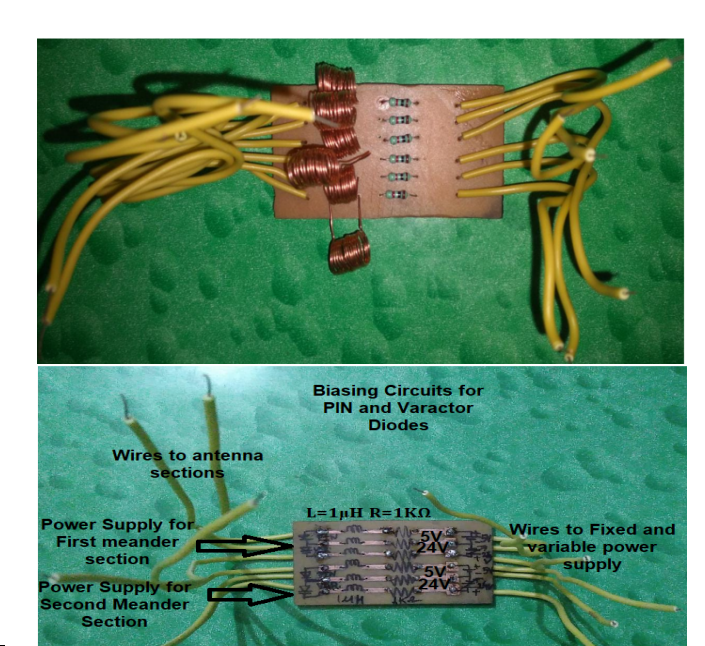


FIGURE 5. Fabricated Active Integrated Antenna (a) prototype front and rear view (b) Diodes biasing circuit front and bottom views

#### IV. RESULTS AND DISCUSSIONS

#### A. Frequency Reconfigured Switching Modes

The frequency reconfigurability of the antenna is achieved by the ON/OFF switching actions of the PIN diodes (D1, D2) in the Meander arms of PIFA. The ON state and OFF state equivalent of each PIN diode (BAR64 02V) are represented in Fig. 6(a). The switching mode of operation depends upon all possible four combinations of ON/OFF cases of two PIN. The reflection coefficients of all four cases concerning the un-reconfigured antenna are compared in Table III and depicted in Fig. 6(b).

# Mode 1: (Both diodes are OFF)

In the case first, with diodes, both diodes are OFF, and the antenna is tuned with four resonance frequencies in three bands. The antenna has excellent gain values 6.71dBi and 1.71dBi, 7.80dBi in the upper (0.78-1.46GHz) and lower (0.78-1.46GHz) band while negative gain of -3.65dBi, in the middle narrow band (1.70-1.74GHz).

#### Mode 2: (D1 OFF and D2 ON)

In the case second with the D1 diode in the OFF state, while the D2 diode is in the ON state, the antenna is tuned with three resonance frequencies in dual bands. The antenna has good gain values 2.29dBi and 3.12dBi in the lower (0.77-1.51GHz) band while excellent 10.32dBi in the upper (2.48-2.82GHz) with decreased reflection coefficient value in the lower band and improved value in the upper band.

Mode of Operation		f <sub>r</sub> (GHz)	-10dB Bands f <sub>L</sub> - f <sub>H</sub> (GHz)	<b>S</b> <sub>11</sub> (dB)	G (dBi)
D1	D2	(GHZ)			
Un-Recor	Un-Reconfigured		0.78-1.01,	-22.30,	5.80,
(PIN Dioc	des are not	1.47	1.34-1.62,	-17.56,	3.45,
Connecte	d)	2.01	1.85-2.18,	-12.67,	-10.26,
		2.57	2.44-2.67,	-17.64,	4.07,
		2.79	2.76-2.80	-16.82	20.44
OFF(0)	OFF(0)	0.86 &	0.78-1.46,	-33.88 &	6.71
		1.29,		-14.81,	&
		1.71,		-15.98,	1.71,
		2.61	1.70-1.74,	-16.71	-3.65,
			2.52-2.71		7.80
OFF(0)	ON(1)	0.86 &	0.77-1.51,	-19.71 &	2.29
		1.34,		-16.72,	&
		2.59		-34.45	3.12,
			2.48-2.82		10.32
ON (1)	OFF(0)	0.86,	0.77-1.51,	-15.83,	7.36,
		1.48,	1.38-1.63,	-15.85,	1.70,
		1.71	1.68-1.75,	-21.67,	-2.75,
		2.57	2.48-2.64	-12.57	1.08
ON (1)	ON (1) ON (1)		0.78-1.02,	-23.33,	7.27,
		1.46,	1.34-1.62,	-17.28,	3.85,
		2.0,	1.72-2.18,	-12.90,	-10.58,
		2.63	2.45-2.71	-40.18	18.18
		ĺ	l		

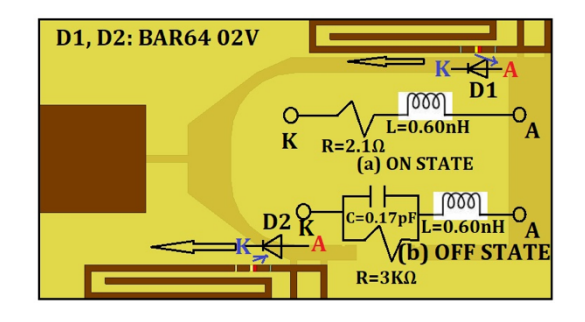
#### Mode 3: (D1 ON and D2 OFF)

In case the third with a D1 diode is in the ON state and the D2 diode is in the OFF state, the antenna is tuned with four resonance frequencies in quad bands. The antenna has excellent gain values 7.36dBi in the lower band (0.77-1.51GHz) and 1.70dBi in the second band, -2.75dBi in the third band (1.68-1.75GHz), and 1.08dBi in the upper (2.48-2.68GHz) band.

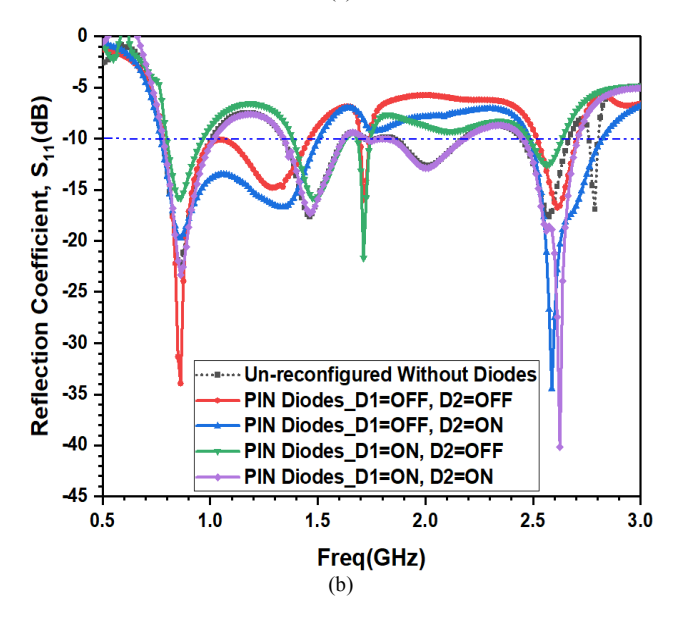
# Mode 4: (Both diodes are ON)

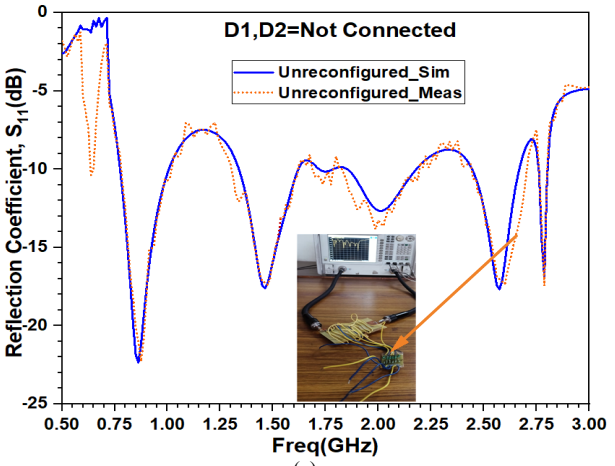
In case the fourth with both diodes is ON, the antenna is tuned with four resonance frequencies in four bands. The antenna has excellent gain values 7.27dBi, 3.85dBi, and 18.18 dBi in the first, second, and fourth bands while the negative gain is at the third resonance frequency of 2.0GHz.

All four reflection coefficients follow the unreconfigured case S11 plot with a change in the lower and upper-frequency band bandwidth and with the elimination of the fifth band. Un-frequency reconfigured antenna measured and simulated results are compared in Fig. 6(c) and all the four switching ON/OFF conditions of the PIN diodes reflection coefficients along with their measured reflection coefficients (with full reverse bias across the Varactor diodes) are represented in the Fig. 6(d). The both the results are found in excellent match.



(a)





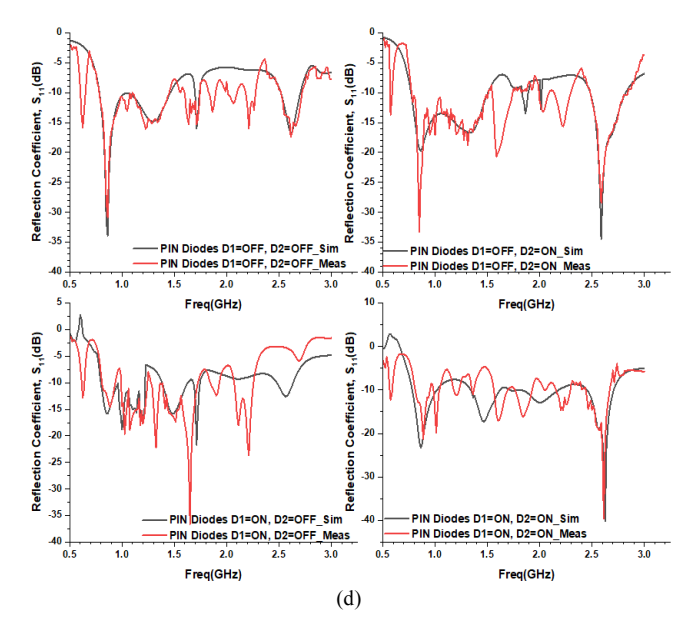


FIGURE 6. (a) PIN diodes (BAR64 02V) switching states (b) Frequency Reconfigure Switching Modes of Antenna (c) Un-frequency reconfigured (d) Frequency reconfigured Modes

VOL. 13, NO. 2, JULY 2024 7



#### B. UWB Sensing with Varactor Diodes

UWB sensing in the antenna is achieved by tuning the Varactor diodes. The tuning of the Varactor diode is achieved by varying the reverse bias voltage across the Varactor diodes (SOD 323/ SMV1702-011LF).

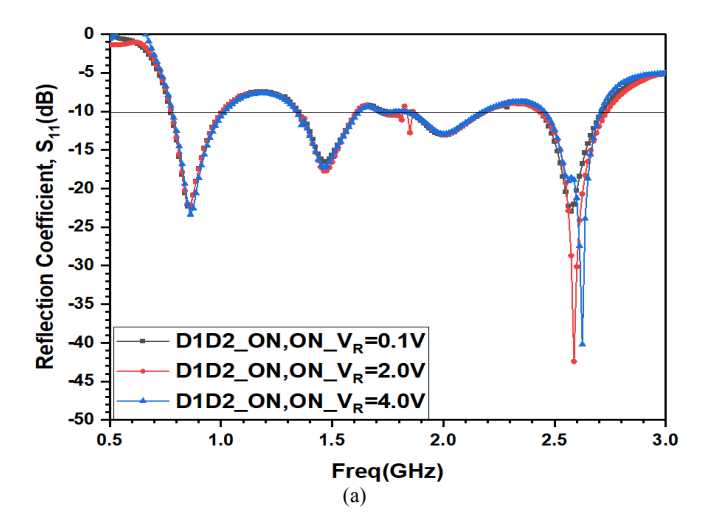
#### Mode 1: (Both PIN diodes are ON)

The variation of reverse voltage across the varactor diodes with both PIN diodes D1 and D2 are in the ON state results in a change in capacitor values. The capacitor values with bias voltage 0.1V, 2V and 4V are 110pF, 50pF and 29pF respectively [29]. The effect of variation of voltage across the Varactor diodes on reflection coefficient plots is represented in Fig. 7(a) and displayed in Table IV. It is observed that the supply voltage variation does not affect the bandwidth and resonance frequencies in noticeable value while it improves the reflection coefficient below -10dB and hence plays a role to improve better impedance matching. The simulated and measured results of both the PIN diodes are in ON situation with variable Varactor diode reverse bias voltages 0.1V, 2V, and 4V are compared in the Fig. 7(b) and these results are found in excellently matched in each case.

TABLE IV. UWB sensing antenna with variable voltage

Mode of Operation D1 D2		f <sub>p</sub> (GHz)	-10dB Bands <b>f</b> <sub>L</sub> - <b>f</b> <sub>H</sub> (GHz)	S <sub>11</sub> (dB)	G (dBi)
ON(1)	ON(1)				
with 0.1	V_110pF	0.86,	0.77-1.01,	-22.32,	4.02,
		1.47,	1.35-1.61,	-16.54,	3.55,
		2.0,	1.83-2.19,	-13.10,	-9.56,
		2.58	2.43-2.72	-22.78	10.09
with 2V	_50pF	0.85,	0.78-1.01,	-22.03,	4.69,
		1.47,	1.34-1.61,	-17.73,	3.90,
		2.0,	1.84-2.19,	-12.96,	2.23,
		2.59	2.43-2.74	-42.42	5.06
with 4V	_29pF	0.86,	0.78-1.02,	-23.33,	7.27,
		1.46,	1.34-1.62,	-17.28,	3.85,
		2.0,	1.72-2.18,	-12.90,	-10.58,
		2.63	2.45-2.71	-40.18	18.18

Note:  $f_r = \text{resonance frequency (GHz)}$ ;  $f_L - f_H = -10 \text{dB}$  lower frequency and Upper frequency (GHz); G = Antenna Gain (dBi);  $S_{11} = Reflection$  Coefficient (dB).



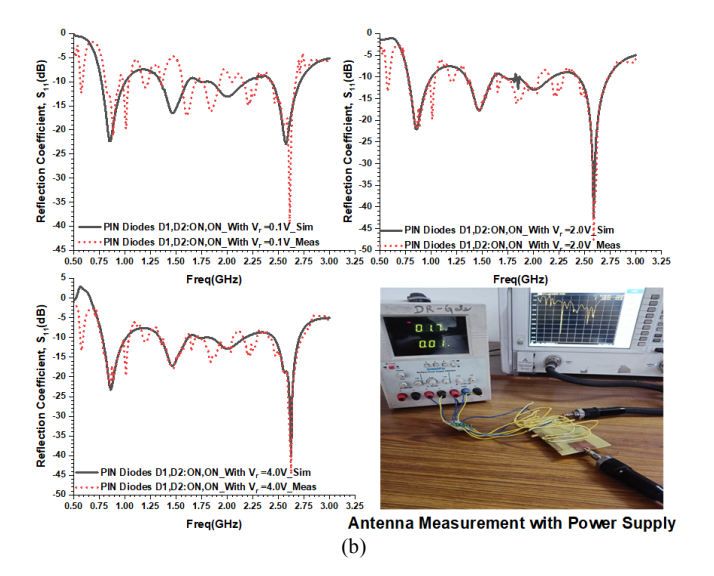


FIGURE 7. UWB sensing with Both PIN diodes in ON states(a) Simulated Reflection Coefficients (b) Simulated vs Measured Reflection Coefficients.

#### Mode 2: (Both PIN diodes are OFF)

In the second mode of operation both the PIN diodes are kept in an OFF state and voltages across the Varactor diodes are varied as 0.1V, 2V, and 4V. The effect of variation of reverse bias voltage on UWB sensing in terms of performance parameter S11 have compared in Fig. 8 (a) and results of the comparison of performance parameters are tabulated in Table V. It is concluded from the table that with OFF state PIN diodes and variation of Varactor reverse voltage jointly combined the lower two bands and results in wide bandwidth instead of narrow bandwidth as in previous case. The middle band where the antenna gain was negative now becomes narrower. The simulated and measured results of both the PIN diodes off situation with variable Varactor diode reverse bias voltages 0.1V, 2V, and 4V are compared in the Fig. 8(b) and these results are found in excellently matched in each case.

TABLE V. UWB sensing with antenna

Mode of	$\mathbf{f_r}$	-10dB	S <sub>11</sub>	G
Operation	(GHz)	Bands	(dB)	(dBi)
D1 D2		$\mathbf{f_L} - \mathbf{f_H}$		
OFF(0) OFF(0)		(GHz)		
with 0.1V_110pF	0.85 &	0.78-1.47,	-36.42	2.90 &
	1.30,		&	4.35,
	1.72,	1.69-1.74,	-14.94,	-2.78,
	2.61,	2.51-2.68,	-15.60,	20.97,
	2.84	2.80-2.90	-21.01,	17.88
			-11.36	
with 2V_50pF	0.85 &	0.78-1.46,	-36.42	3.68 &
	1.30,		&	3.06,
	1.72,	1.70-1.74,	-14.94,	-3.29,
	2.61	2.53-2.70	-15.60,	6.64,
			-14.62	
with 4V_29pF	0.86 &	0.78-1.46,	-33.88	6.71 &
	1.29,		&	1.71,
	1.71,	1.70-1.74,	-14.81,	-3.65,
	2.61	2.52-2.71	-15.98,	7.80
			-16.71	



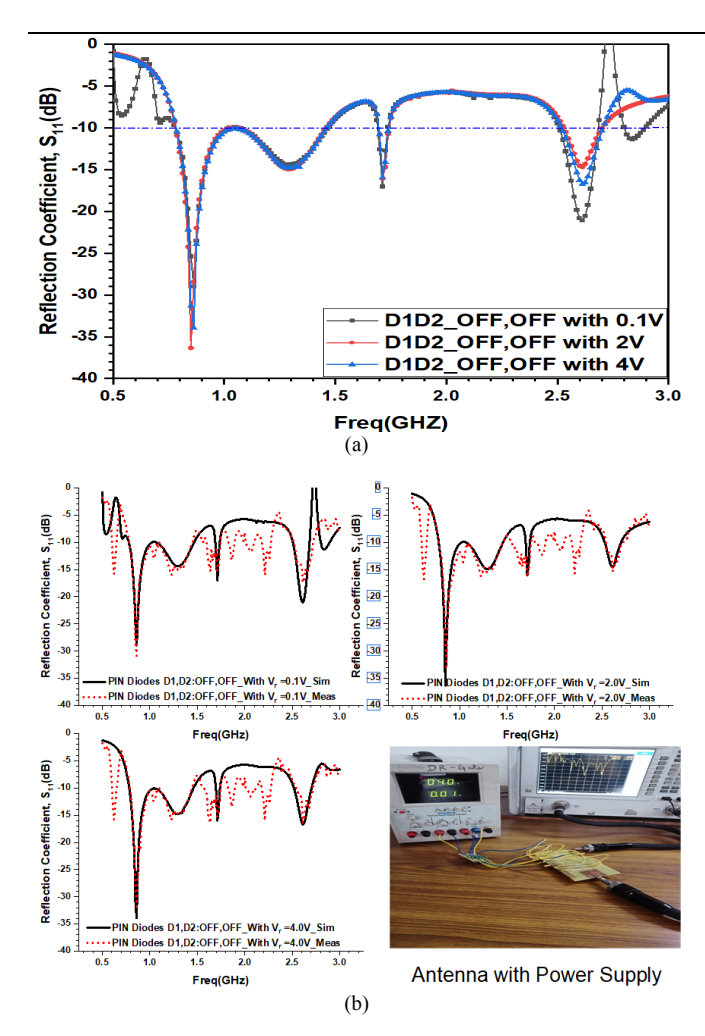


FIGURE 8. UWB sensing with Both PIN diodes in OFF states (a) Simulated Reflection Coefficients (b) Simulated vs Measured Reflection Coefficients

#### C. Variation of Capacitors of Varactor Diodes

TABLE VI. UWB sensing tuning with capacitive Effect

Mode of	f	f <sub>r</sub>	-10dB Bands	S <sub>11</sub>	G
Operati	on	(GHz)	$f_L - f_H$	(dB)	(dBi)
D1	D2		(GHz)		
ON(1)	ON(1)				
1pF		0.86,	0.78-1.78,	-26.46,	3.17,
		1.43 &		-22.12	3.47
		1.65,		&	&
		2.03		-23.19,	-2.90,
		2.59	1.94-2.14	-10.74,	-11.21,
			2.45-2.71	-17.80	7.45
3pF		0.86,	0.78-1.08,	-25.33,	5.98,
1		1.46,	1.30-1.80,	-30.19,	3.83,
		2.01,	1.87-2.17,	-12.02,	-10.62,
		2.58	2.45-2.72	-17.25	1.69
5pF		0.86,	0.78-1.05,	-25.12,	5.41,
1		1.46,	1.32-1.65,	-22.45,	3.91,
		2.01,	1.90-2.19,	-12.50,	-10.65,
		2.58	2.44-2.69	-17.94	9.91
7pF		0.86,	0.78-1.03,	-23.26,	4.18,
_		1.46,	1.33-1.80,	-20.34,	3.76,
		2.0,	1.85-2.19,	-12.57,	-9.49,
		2.58	2.44-2.66,	-17.46,	9.10,
		2.84	2.81-2.87	-11.53	13.72
9pF		0.86,	0.79-1.03,	-22.93,	5.03,
		1.46,	1.33-1.79,	-19.73,	3.87,
		2.0,	1.85-2.20,	-12.94,	-9.17,
		2.57	2.42-2.66	-17.86	12.06

The capacitor value of the Varactor diode decreases with an increase in reverse biasing. The reflection coefficient S11 values have been compared in Fig. 9 and arranged in Table VI. It is concluded that deceases value of the capacitor results in fine-tuning, improved matching, widen bandwidth, the improved value of reflection coefficient below -10dB, and helps to eliminate the negative gain mid-band (1.94-2.14GHz) near 2.0 GHz resonance frequency.

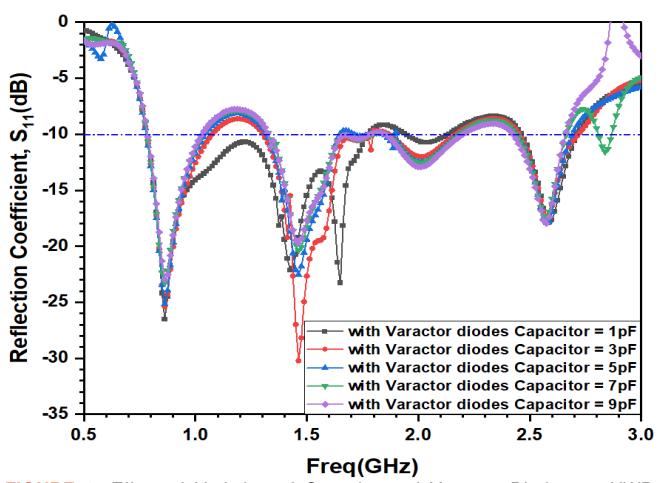


FIGURE 9. Effect of Variation of Capacitors of Varactor Diodes on UWB sensing tuning with capacitive effect

# D. MIMO Diversity Parameters

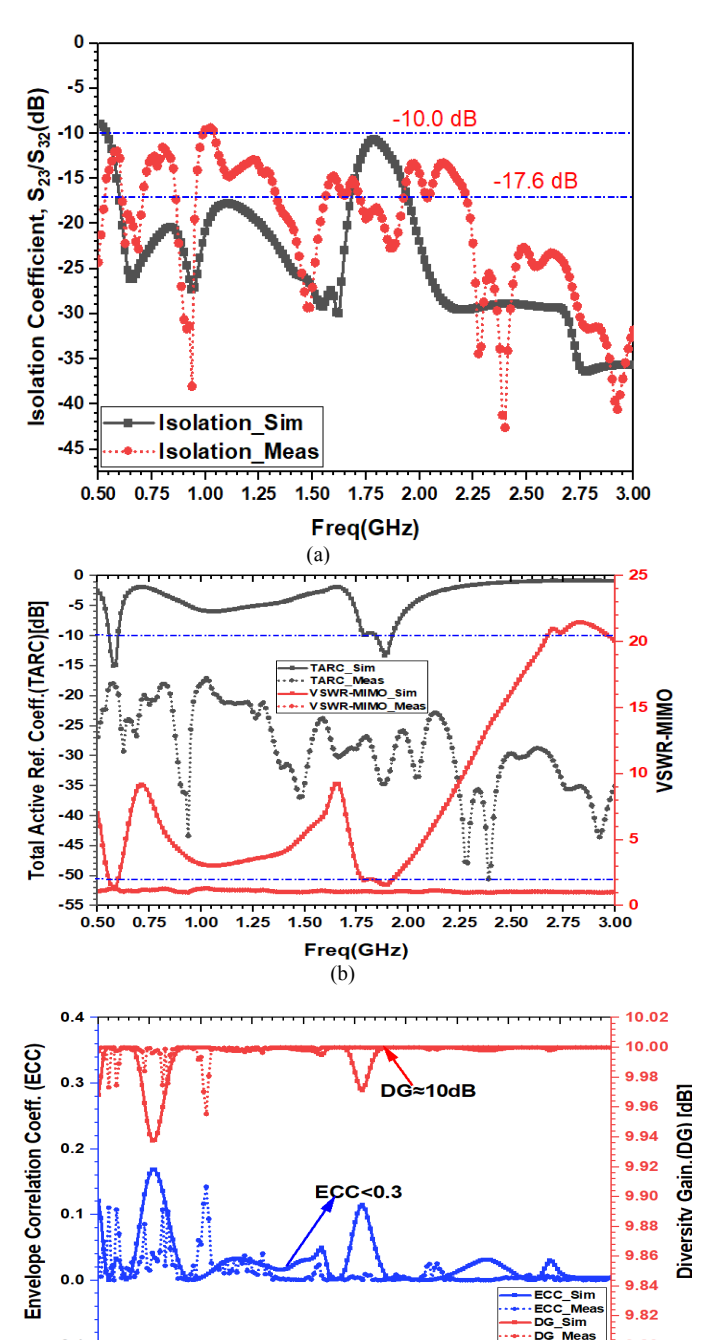
The simulated and measured isolation coefficients in Fig. 10(a) are well below -10dB ensures that both meandered line PIFA elements are excellently coupled. The measured Total Active Reflection Coefficients (TARC) and VSWR-MIMO are well lower than -15dB and 2, respectively [Fig. 10(b)] of the fabricated meander line PIFA elements. This yields the fabricated MIMO performs much excellently than the simulated one. Both simulated and measured Envelope Correlation Coefficients (ECC) and Diversity Gain (DG) are lower than 0.3 and close to 10dB respectively as shown in Fig. 10(c), the measured and simulated Mean effective gain (MEG) is lies between ±3dB as shown in Fig. 10(d) and Cross-Correlation Coefficients (CCC) is lower than 0.2 in the most of the interested frequency band as depicted in the Fig. 10(e). The multiplexing efficiency is more than 99% over entire band except 1.7GHz to 1.9GHz as displayed in Fig. 10(f). All the 2X2 MIMO simulated and measured diversity parameters of the two PIFA with meandered line elements have displayed in Fig. 10(a-f) and summarized resultant parameters are arranged in Table VII. The entire resultant parameters are falls within the limits that make the proposed antenna suitable for the use of MIMO operations and functioning.

TABLE VII. Diversity parameters of UWB sensing MIMO

Diversity Parameter	Values
Spatial Distance (D)	49.2mm
Total Active Reflection Coefficient, TARC (<0 dB)	(i) -15.09dB at 0.575GHz, -10dB BW:0.55-0.60GHz (ii) -13.32dB at 1.89GHz
Voltage Standing Wave Ratio, VSWR (< 2)	-10dB BW:1.84-1.93GHz (i) 1.42 at 0.575GHz, Impedance BW: 0.55-0.606GHz



	(ii) 1.9 at 1.89GHz Impedance BW:
	1.78-1.93GHz
Isolation Coefficient (S <sub>23</sub> /S <sub>32</sub> )	<-17.6dB for full UWB sensing 0.5
	to 3.0GHz
	except BW: 1.68-1.95GHz (where -
	$17.6dB \ge S_{23} \le -10dB$ )
Envelope Correlation Coefficient,	<0.17 (the proposed MIMO is
ECC (<0.3)	excellent to use for MIMO
ECC (<0.3)	excellent to use for MIMO operation)
ECC (<0.3)  Diversity Gain, DG [dB]	***************************************
, ,	operation)
Diversity Gain, DG [dB]	operation) Close to 10 dB (i.e. <10dB)

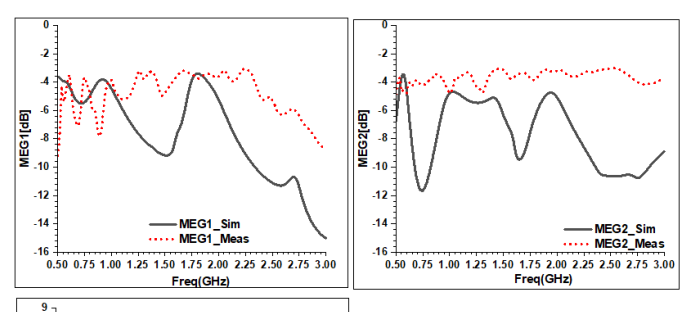


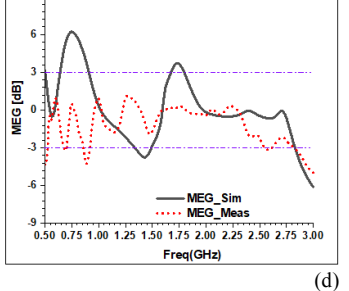
1.75 2.00 2.25 2.50

0.75 1.00 1.25

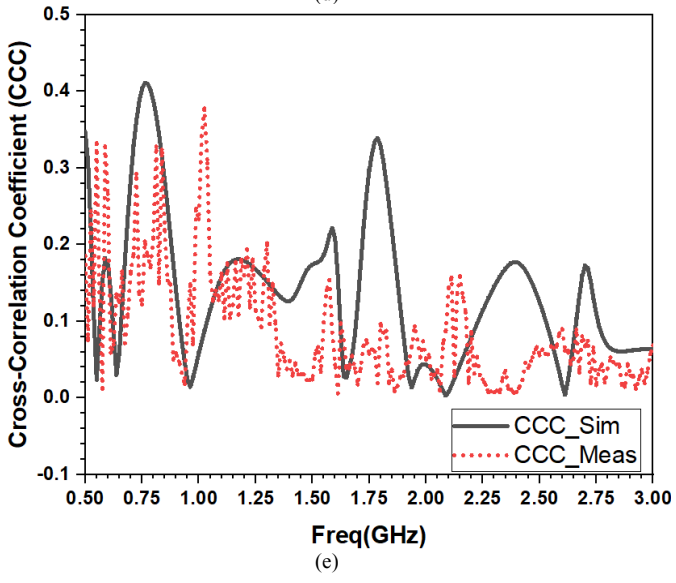
1.50

Freq(GHz) (c)





-3dB< MEG <+3dB



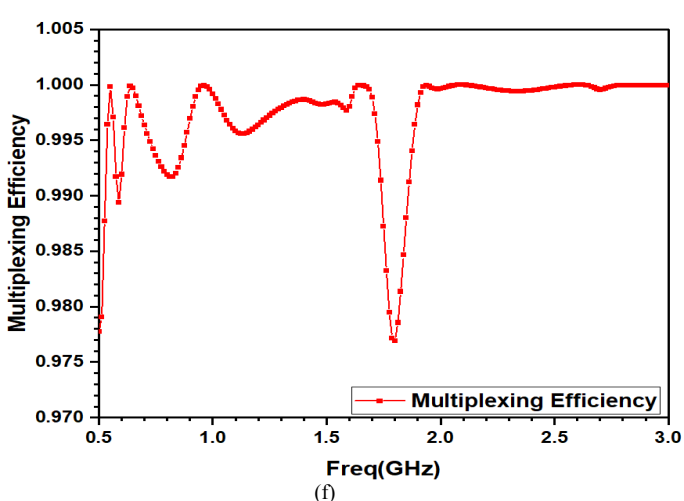


FIGURE 10. UWB sensing MIMO Antenna Diversity Parameters (a) Isolation Coefficient, (b) TARC and VSWR, (c) ECC and DG, (d) MEG, (e) CCC, and (f) Multiplexing Efficiency (¶Mux)

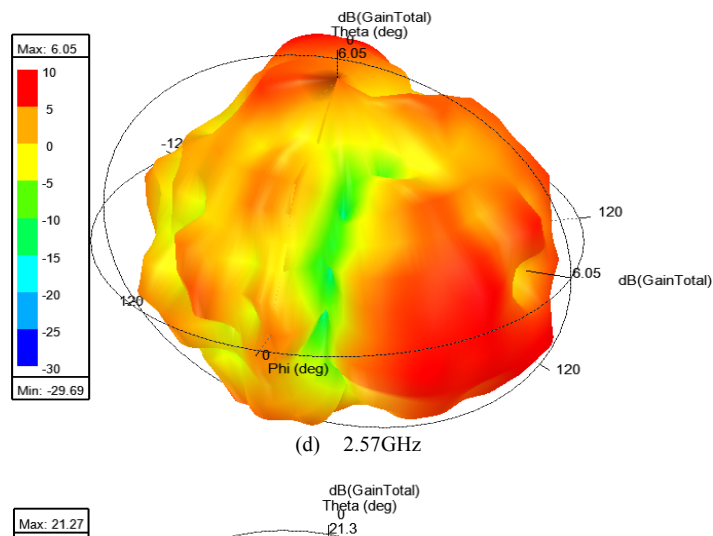
10 VOL. 13, NO. 2, JULY 2024

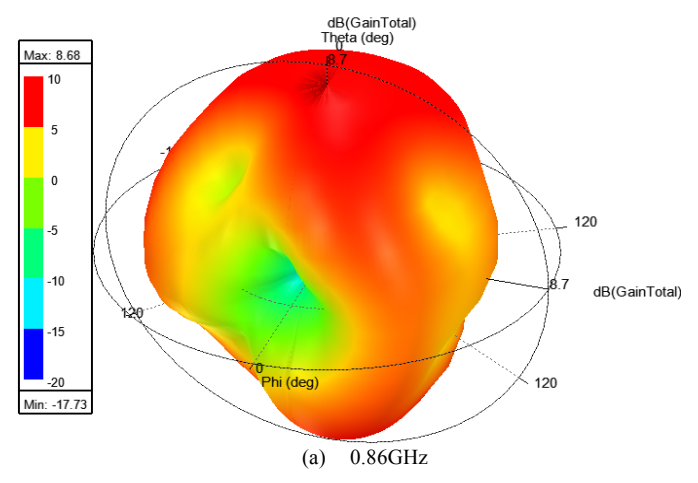
2.75 3.00

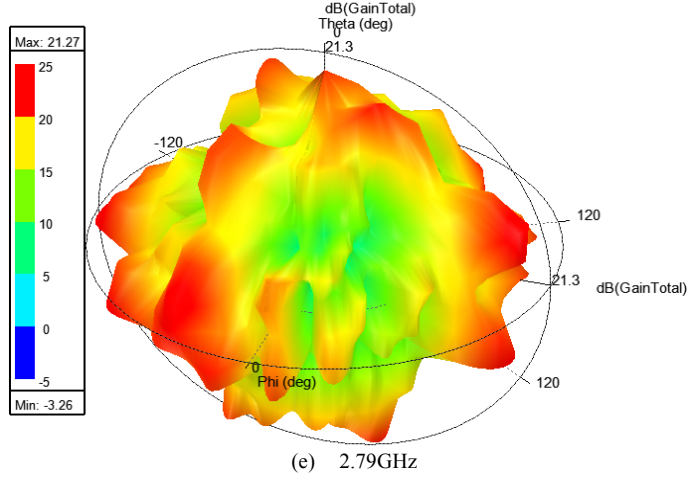


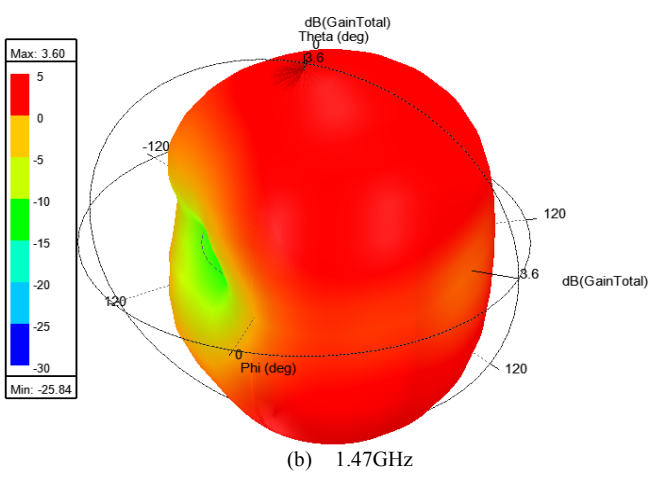
# E. Antenna Radiation Patterns

The 3D radiation patterns of the gain are displayed in Fig. 11(a-e) at five frequencies: 0.86 GHz, 1.47 GHz, 2.01 GHz, 2.57 GHz, and 2.79 GHz. The maximum peak gain values at these resonance frequencies are 8.68 dB, 3.60 dB, 4.31 dB, 6.05 dB, and 21.27 dB, respectively. The radiation gain polar patterns in the E-plane with a phi angle ( $\Phi$ =0°) and the polar patterns in the H-plane with a phi angle ( $\Phi$ =90°) at the five resonance frequencies are illustrated in Fig. 12. In all cases, the antenna exhibits either bidirectional or omnidirectional radiation patterns. This supports the idea that the antenna is a strong candidate for use in Cognitive Radio (CR) applications. Simulated and measured radiation patterns in E-planes and H-planes are found in excellent agreement.







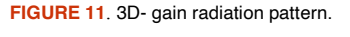


dB(GainTotal) Theta (deg)

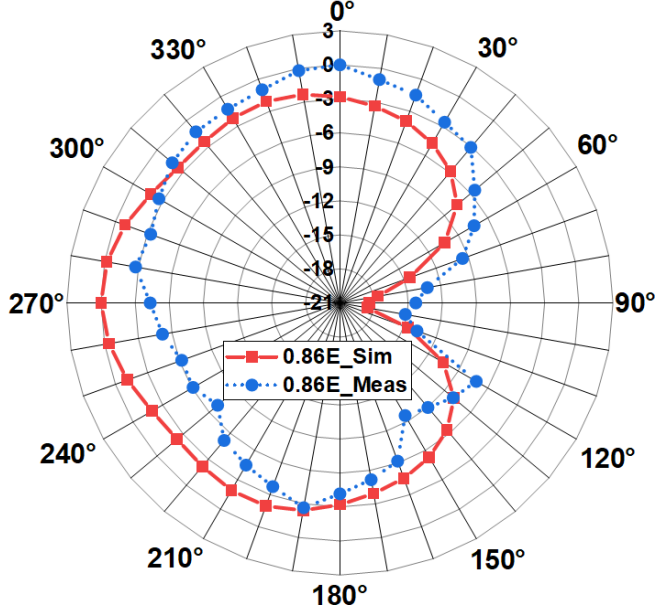
2.01GHz

Max: 4.31

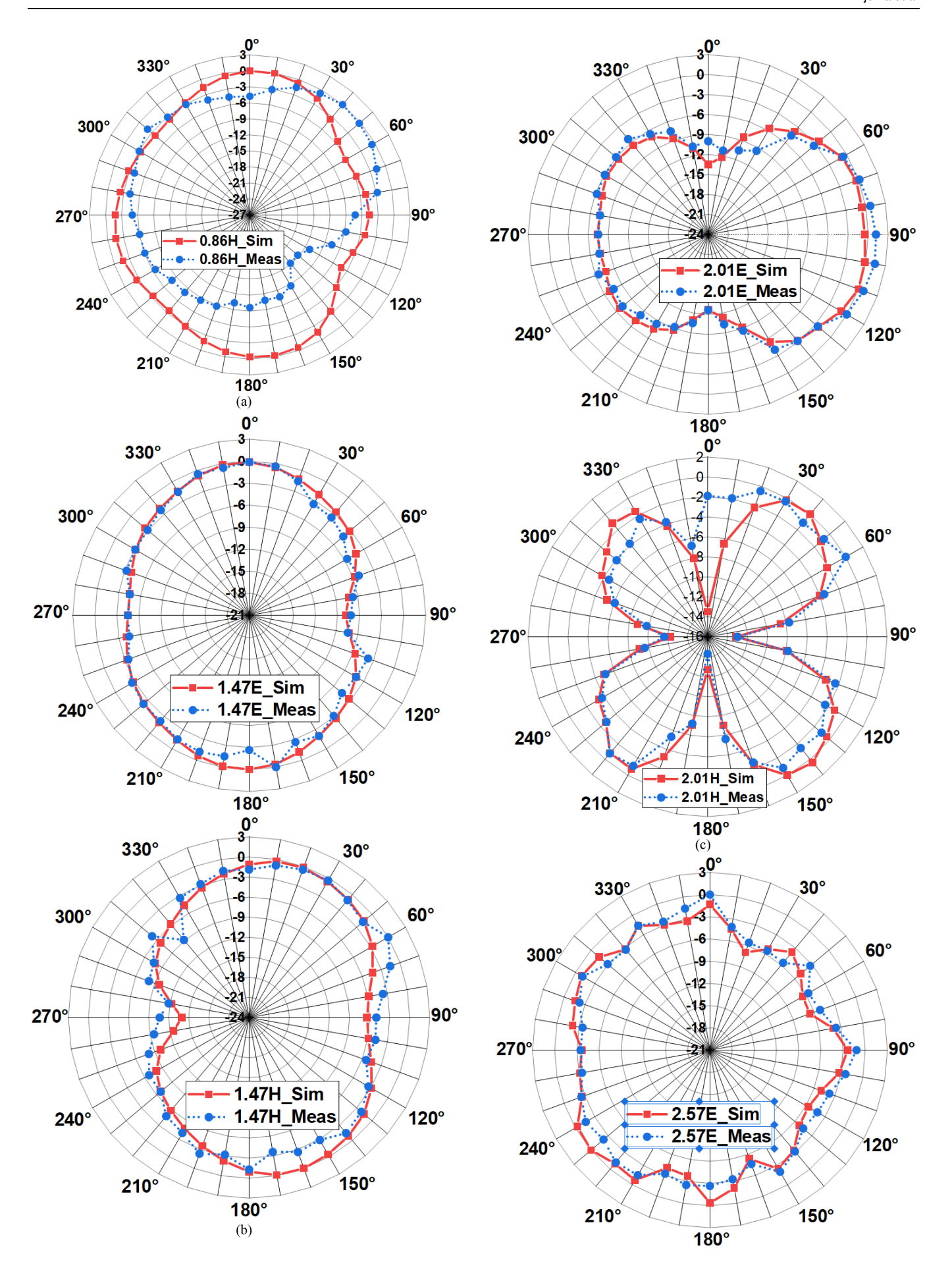
-10 -15













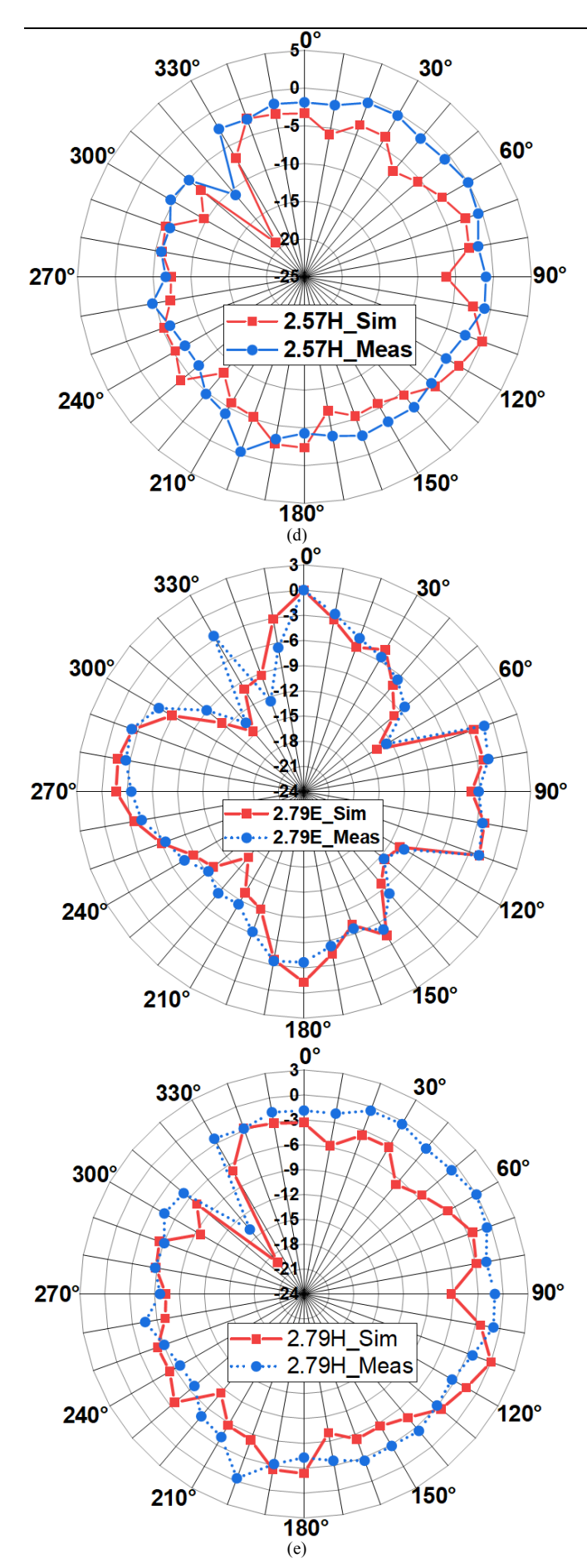


FIGURE 12. E-plane and H-plane gain radiation polar patterns

#### F. Antenna Gain

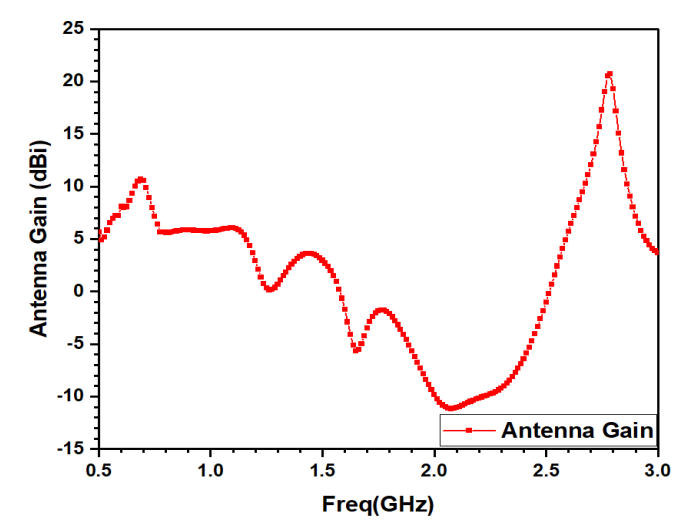


FIGURE 13. Gain of UWB sensing Antenna

The proposed antenna gain against the frequency sweep from 0.5GHz to 3.0GHz is presented in Fig. 13. It is noticed that the antenna gain is more than 5dBi stable gain for a frequency range from 0.5GHz to 1.2GHz. This makes the antenna suitable for use in lower ISM band applications at the 915MHz band. The antenna has a negative gain from 1.6 GHz to 2.4 GHz. The interesting fact is that not much application exists within this range of frequency bands. From 2.4GHz to 3GHz the antenna gain is extremely high and reaches its peak value of 22 dBi at 2.70GHz.

# G. Axial Ratio (AR) and Polarization

The axial ratio (AR) plot is crucial for detecting polarization, as illustrated in Fig. 14 for the proposed antenna. It is observed that the UWB sensing antenna maintains an axial ratio of less than 3 dB within specific frequency bands: 0.5 GHz to 0.55 GHz, 0.78 GHz to 0.89 GHz, 1.84 GHz to 1.88 GHz, and 2.40 GHz to 2.48 GHz. This ensures circular polarization characteristics within these ranges. Conversely, outside of these bands, the AR value exceeds 3 dB, indicating linear polarization behavior. Consequently, the proposed UWB sensing antenna is dual-polarized

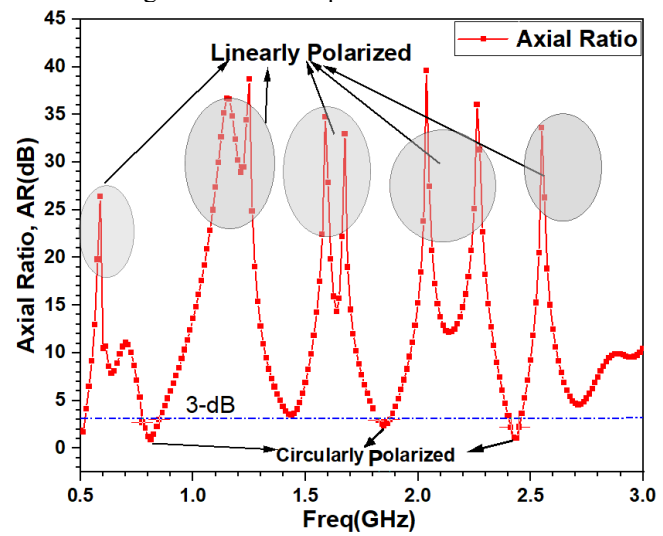




FIGURE 14. Axial Ratio and Polarization

#### H. State-of-Art Comparison

The closely existing literature antennas have been arranged in Table VIII and their resultant parameters are compared with the proposed UWB sensing frequency reconfigurable antenna. In the proposed work all MIMO performance parameters have been analyzed. MIMO PIFA with meandered line elements is placed at offset locations. As compared to all other UWB sensing antennas the proposed antenna has five bands and excellent gain and multiplexing efficiency.

TABLE VIII. Antenna comparison table

Ref.	Ant. Size	UWB	N	G	η	MIMO	CR
	(mm <sup>3</sup> )	Sensi	and	(dBi)	(%)	(Parameters)	Enabled
		ng	-10dB				Applica
		(GHz)					tions
			<b>f<sub>L</sub> − f<sub>H</sub></b> (GHz)				
[5]	60x120x1.5	Yes	4	3.2	81	Yes	Yes
2018						3X3 MIMO	
						ECC<0.248	
						TARC=-17dB	
						Tuned over 1.77-	
[(1	50x90.5x0.76	Yes	2	14.17	60	7.65GHz. Yes	No
[6] 2016	50X90.5X0.76	Yes	2	14.1/	60	2X2 MIMO	NO
2010						ECC<0.33	
						DG=9.5dB	
						Isolation<-12d	
						В	
[7]	60x120x1.5	Yes	1	3.98	92.5	Yes	Yes
2019						2X2 MIMO 0.9-2.6GHz	
						ECC<0.19	
						Isolation<—12.5	
						dB	
[8]	150x200x0.76	No	3	3.52	84	Yes	Yes
2019						2X2 MIMO	
						ECC<0.143	
						Isolation<—14d	
						В	
[9]	60x120x1.56	Yes	3	2.98	44.67	Yes	Yes
2013						2X2 MIMO(Inline)	
						ECC<0.078	
						Isolation <ng< td=""><td></td></ng<>	
[10]	85x85 x1.5	Yes	1	6.15d	NG	No	Yes
2017				Bi			
[11]	80x70 x1.6	No	3	NG	74	Yes	Yes
2014	120 2 2 2						
[12]	120x6 0x1.6	Yes	3	4.0	NG	Yes	Yes
2022						2X2 MIMO (Inline)	
						ECC: NG	
						Isolation<-10dB	
Propo	120×6 0×1.6	Yes	5	6.73	99.72	Yes	Yes
sed						2X2 MIMO	

## V. CONCLUSION

Advanced Ultra-Wideband (UWB) sensing techniques for frequency-reconfigurable Multiple Input Multiple Output

(MIMO) antenna design have been tested and analyzed in this work. The designed antenna is dual-polarized, both linearly and circularly, with stable gain, reflection coefficient, and consistent resonance frequencies to meet the requirements of Cognitive Radio applications. The PIN diodes are connected for reconfigurable operation with a mirror-shaped slotted sensing antenna, covering a frequency band ranging from ~770 to 2800MHz. The frequency-reconfigured switching modes may vary the fractional bandwidth of existing bands from narrowband to wideband, making the same antenna suitable for multiple applications. UWB sensing and tuning have been achieved by Varactor diodes, supporting improvement in impedance matching and reflection coefficient values lower than -10dB. A peak gain of 18.18 dBi for ON conditions of the PIN diodes is observed from the gain plot, while 6.71 dBi for diodes OFF conditions. Separate biasing circuits have been designed for the reconfigurable UWB sensing MIMO active antenna to reduce the parasitic and mutual coupling effects of the components. The paper also considered all MIMO parameters within the standard specified values, ensuring that the proposed antenna is wellsuited for MIMO operation. MIMO elements are placed at offset locations to improve the isolation coefficient or decoupling factor. The differences between the measured and simulated results are due to errors in the SMA connectors, PIN diodes, Varactors, and DC blocking capacitors soldering issues, as well as fabrication and measurement errors. Because the large area on the top side and bottom is free from copper, this area could be used for the connection of the power supply and biasing arrangement on the same PCB board in the future. The proposed antenna could be easily deployed in baby toys, drone applications, Global Network Satellite System (GNSS) for GPS tracking, smartphones, and modern televisions for Witablets, laptops, Fi/WLAN/ISM band applications. Such co-designed antenna techniques improve the MIMO performance and also reduce and simplify the tedious computational optimization and analysis of the antenna geometries that are of utmost interest in present RF System design.

# **ACKNOWLEDGMENT**

The author would like to thank the Centre for Excellence in Microwave Engineering, Osmania University, Hyderabad, India.

# REFERENCES

- [1] A.Varshney, V. Sharma, "A comparative study of microwave rectangular waveguide-to-microstrip line transition for millimeter wave, wireless communications, and radar applications," in Microwave Review, vol. 26, no. 2, pp. 21-37, Dec. 2020.
- [2] T.Vijetha, D.Rama Krishna, K.Barath "Design and analysis of triband monopole ultra wide band (UWB) antenna" in Telecommunications and Radio Engineering, vol 82, pp.51-67,Dec.2023
- [3] A. Varshney, V. Sharma, "An Inline V-Band WR-15 Transition Using Antipodal Dipole Antenna as RF Energy Launcher@ 60 GHz for Satellite Applications," in Electronics, vol. 11, no. 23, article 3360, Nov. 2022.
- [4] P.S. Evangelin, T. M. Neebha, A. D. Andrushia, J. Roopa Jeyasingh, A. Varshney, X. Anitha Mary, "Design and Analysis of Meander



- Slitted Monopole Antenna for Wireless Application," 6th International Conference on Devices, Circuits, and Systems (ICDCS), pp. 480-483, April 2022.
- [5] R. Hussain, M. S. Sharawi and A. Shamim, "An Integrated Four-Element Slot-Based MIMO and a UWB Sensing Antenna System for CR Platforms," in *IEEE Transactions on Antennas and Propagation*, vol. 66, no. 2, pp. 978-983, Feb. 2018.
- [6] S. K. Dhar, M. S. Sharawi, O. Hammi and F. M. Ghannouchi, "An Active Integrated Ultra-Wideband MIMO Antenna," in IEEE Transactions on Antennas and Propagation, vol. 64, no. 4, pp. 1573-1578, April 2016.
- [7] X. Zhao, S. Riaz and S. Geng, "A Reconfigurable MIMO/UWB MIMO Antenna for Cognitive Radio Applications," in IEEE Access, vol. 7, pp. 46739-46747, 2019.
- [8] R. Hussain and M. S. Sharawi, "An Integrated Slot-Based Frequency-Agile and UWB Multifunction MIMO Antenna System," in IEEE Antennas and Wireless Propagation Letters, vol. 18, no. 10, pp. 2150-2154. Oct. 2019.
- [9] R. Hussain and M. S. Sharawi, "A Cognitive Radio Reconfigurable MIMO and Sensing Antenna System," in IEEE Antennas and Wireless Propagation Letters, vol. 14, pp. 257-260, Oct. 2015.
- [10] Sharma, S., & Tripathi, C. C," A Novel Reconfigurable Antenna with Spectrum Sensing Mechanism for CR System," *Progress in Electromagnetics Research C*, Vol. 72, 187–196, March. 2017.
- [11] Y. Tawk, J. Costantine, and C. G. Christodoulou, "Reconfigurable Filtennas and MIMO in Cognitive Radio Applications," in IEEE Transactions on Antennas and Propagation, vol. 62, no. 3, pp. 1074-1083, March. 2014.
- [12] A. Varshney, T. M. Neebha, V. Sharma, J. G. Jency, A. D. Andrurshia, "Dodecagon-Shaped Frequency Reconfigurable Antenna Practically Loaded with 3-Delta Structures for ISM Band and Wireless Applications," IETE Journal of Research, Published online (2022)1-13. https://doi.org/10.1080/03772063.2022.2034536.
- [13] T. Vijetha, R. K. Dasari, "A Frequency Reconfigurable MIMO Antenna with UWB Sensing for Multi-Band Operations," International Journal of Microwave and Optical Technology, Vol.18, no.1, 2022, pp.57-68.
- [14] N. H. Chamok, M. H. Yılmaz, H. Arslan and M. Ali, "High-Gain Pattern Reconfigurable MIMO Antenna Array for Wireless Handheld Terminals," in *IEEE Transactions on Antennas and Propagation*, vol. 64, no. 10, pp. 4306-4315, Oct. 2016.
- [15] H. Li, B. K. Lau, and S. He, "Design of Closely Packed Pattern Reconfigurable Antenna Array for MIMO Terminals," in IEEE Transactions on Antennas and Propagation, vol. 65, no. 9, pp. 4891-4896, Sept. 2017.
- [16] R. Hussain, A. Ghalib, and M. S. Sharawi, "Annular Slot-Based Miniaturized Frequency-Agile MIMO Antenna System," in IEEE Antennas and Wireless Propagation Letters, vol. 16, pp. 2489-2492, July. 2017.
- [17] R. Hussain, M. U. Khan and M. S. Sharawi, "An Integrated Dual MIMO Antenna System With Dual-Function GND-Plane Frequency-Agile Antenna," in IEEE Antennas and Wireless Propagation Letters, vol. 17, no. 1, pp. 142-145, Jan. 2018.

- [18] N. Haider, A. G. Yarovoy and A. G. Roederer, "\$L/S\$ -Band Frequency Reconfigurable Multiscale Phased Array Antenna With Wide Angle Scanning," in *IEEE Transactions on Antennas and Propagation*, vol. 65, no. 9, pp. 4519-4528, Sept. 2017.
- [19] B. Liu, J. Qiu, S. Lan, H. Zong, and N. Wang, "Pattern Reconfigurable Dielectric Resonator Antenna Actuated by Shorted Parasitic Elements," 2019 IEEE International Symposium on Antennas and Propagation and USNC-URSI Radio Science Meeting, pp. 77-78, Oct.2019.
- [20] M. -C. Tang, Z. Wen, H. Wang, M. Li and R. W. Ziolkowski, "Compact, Frequency-Reconfigurable Filtenna With Sharply Defined Wideband and Continuously Tunable Narrowband States," in IEEE Transactions on Antennas and Propagation, vol. 65, no. 10, pp. 5026-5034, Oct. 2017.
- [21] R. Hussain, M. S. Sharawi and A. Shamim, "4-Element Concentric Pentagonal Slot-Line-Based Ultra-Wide Tuning Frequency Reconfigurable MIMO Antenna System," in IEEE Transactions on Antennas and Propagation, vol. 66, no. 8, pp. 4282-4287, Aug. 2018.
- [22] L. Sumana, E. F. Sundarsingh and S. Priyadharshini, "Shape Memory Alloy-Based Frequency Reconfigurable Ultrawideband Antenna for Cognitive Radio Systems," in *IEEE Transactions on Components*, Packaging, and Manufacturing Technology, vol. 11, no. 1, pp. 3-10, Jan. 2021.
- [23] L. Xing et al., "A High-Efficiency Wideband Frequency-Reconfigurable Water Antenna with a Liquid Control System: Usage for VHF and UHF Applications," in IEEE Antennas and Propagation Magazine, vol. 63, no. 1, pp. 61-70, Feb. 2021.
- [24] X. Zhang, Y. Li, W. Wang, and W. Shen, "Ultra-Wideband 8-Port MIMO Antenna Array for 5G Metal-Frame Smartphones," in IEEE Access, vol. 7, pp. 72273-72282, May. 2019.
- [25] Ghaffar, A.; Li, X.J.; Awan, W.A.; Iffat Naqvi, S.; Hussain, N.; Seet, B.-C.; Alibakh shikenari, M.; Falcone, F.; Limiti, E," Design and Realization of a Frequency Reconfigurable Multimode Antenna for ISM, 5G-Sub-6-GHz, and S-Band Applications," Appl. Sci. 11, pp.16-35, Feb. 2021.
- [26] R. Hussain, M. U. Khan, and M. S. Sharawi, "Design and Analysis of a Miniaturized Meandered Slot-Line-Based Quad-Band Frequency Agile MIMO Antenna," in IEEE Transactions on Antennas and Propagation, vol. 68, no. 3, pp. 2410-2415, March. 2020.
- [27] S. R. Thummaluru, M. Ameen and R. K. Chaudhary, "Four-Port MIMO Cognitive Radio System for Midband 5G Applications," in IEEE Transactions on Antennas and Propagation, vol. 67, no. 8, pp. 5634-5645, Aug. 2019.
- [28] X. -T. Yuan, W. He, K. -D. Hong, C. -Z. Han, Z. Chen and T. Yuan, "Ultra-Wideband MIMO Antenna System With High Element-Isolation for 5G Smartphone Application," in IEEE Access, vol. 8, pp. 56281-56289, March. 2020.
- [29] Data Sheet SOD-323, "SMV1702-011LF Hyperabrupt Junction Tuning Varactor," Skyworks. www.skyworksinc.com